Impact of Connectivity on Energy Consumption and Battery Life for Electric Vehicles

Wesley D. Connor, Yongqiang Wang, Andreas A. Malikopoulos, *Senior Member, IEEE*, Suresh G. Advani, and Ajay K. Prasad

***Abstract*—Connected vehicle technologies present new opportunities to minimize energy consumption in vehicles. Much of the prior work has focused on the impact of vehicle-to-infrastructure (V2I) communication on energy savings. Here, we analyze the impact of connectivity on both energy savings and battery degradation reduction for an electric bus. Dynamic programming is employed to optimize the velocity profile of a single electric bus passing through a traffic intersection under a V2I regime wherein the intersection timing of the traffic light is known a priori. The optimization seeks to minimize the overall cost function consisting of the electric energy consumption and battery degradation. Simulations have been conducted for both the connected vehicle case and the baseline case without connectivity. Three different battery sizes were investigated, and the results indicate that connectivity confers the greatest cost savings for the smallest battery. An overall cost savings of 27% can be realized by using connectivity to reduce both energy consumption and battery degradation.**

***Index Terms*—Connected vehicles, vehicle-to-infrastructure (V2I), velocity optimization, battery degradation, cost optimization, electric bus.**

I. Introduction

A. Motivation

CLIMATE change concerns have been increasing dramatically in the past few decades. Alternative, cleaner sources of energy for vehicular propulsion are being utilized and tested. Electric vehicles are at the forefront of these alternative energy transportation options. One current challenge is in creating a practical and low-cost electric vehicle. Practicality is constrained by battery recharge time, which decreases vehicle availability. Large battery costs, either upfront or for replacement at its end-of-life, can restrict electric vehicle purchases, especially for electric buses. Thus, there is significant demand for solutions, such as optimal power management systems that can minimize electric energy consumption while extending battery life. In particular, vehicle connectivity can be exploited for this purpose. The next section provides background on work previously conducted in similar areas with and without connectivity and serves to give perspective on its impact on energy reduction.

Manuscript received June 12, 2019; revised February 14, 2020, June 30, 2020, and September 14, 2020; accepted October 10, 2020. Date of publication October 21, 2020; date of current version February 24, 2021. This work was supported by the Federal Transit Administration. *(Corresponding author: Ajay K. Prasad.)*

The authors are with the Department of Mechanical Engineering, University of Delaware, Newark, DE 19716 USA (e-mail: wconnor@udel.edu; sailor@udel.edu; andreas@udel.edu; advani@udel.edu; prasad@udel.edu).

Color versions of one or more of the figures in this article are available online at https://ieeexplore.ieee.org.

Digital Object Identifier 10.1109/TIV.2020.3032642

B. Background

Most of the research in this area has focused on determining an optimal controller when signal timing and stops are unknown resulting in a random nature to vehicle travel. One challenge of creating a real-time optimal control strategy for the power management of vehicles is the computational load. Many have developed strategies which use a limited, rather than infinite, time horizon. LiHong *et al.* [1] proposed an optimized equivalent consumption minimization strategy (ECMS), in which an optimization window of 100 seconds was used. The profiles of several vehicles with vehicle-to-vehicle (V2V) communication were created in a simulation to compare the limited-time horizon optimized ECMS to the ideal case of the infinite time horizon ECMS. A previously established method of Adaptive-ECMS was used as a baseline. To further optimize, the equivalent factors (EFs) for different driving cycles were updated by information from the connected vehicle system. The simulations run using this method compared to the A-ECMS resulted in an average improvement of 1.63%.

In another effort in this area related to real-time controllers dealing with random traffic patterns, Liu and Peng [2] applied a Stochastic Dynamic Programming (SDP) approach as well as an ECMS to the Toyota hybrid system and compared each to the ideal case given by Dynamic Programming (DP) results. City and highway driving cycles were used in the simulation of the study, and for the city cycle, the SDP and ECMS had a larger improvement from the rule-based controller than for the highway cycle. Han and Park [3] developed a method for updating the EF of the ECMS to prolong the lifetime of the battery. By assigning a higher cost to battery SOC far from the initial value, a decrease in the depth of cycles and a longer predicted battery lifetime were achieved. Lin *et al.* [4] applied an SDP to a diesel hybrid truck. This approach provided an implementable design path, allowing control strategies from the SDP to be incorporated into an online control strategy to improve energy management.

In another stochastic embodiment, Vagg *et al.* [5] applied an SDP to a light commercial vehicle to reduce powertrain stress. By applying the stochastic method, the researchers demonstrated a 13% reduction in powertrain stress, quantified by lower peak current demands of the battery and the electric motor. In another

effort [6], the evolution of the state in a series hybrid electric vehicle was modeled as a controlled Markov chain and the control algorithm derived optimal control policy in real time yielding a 6% improvement in fuel consumption. Later on, formulating a multi-objective optimization problem, it was shown that the control policy yielding the Pareto optimal solution minimizes online the long-run expected average cost [7]. The effectiveness of the efficiency of this approach was demonstrated in simulation and it was shown that the Pareto control policy is an optimal control policy that can optimize in real time the power management control of HEVs/PHEVs.

Several research efforts have addressed the optimal control problem of a fuel cell powertrain. These efforts have focused on optimizing the State of Charge (SOC) of the on-board battery, in addition to running the fuel cell stack at a level which minimizes fuel consumption and maximizes the lifetime of the device. Kim and Peng [8] create a power management controller by using SDP results to create a "Pseudo SDP controller." This allows for online control due to reduced computation time, using fewer variables than the full SDP. In addition, the study delineates the degree of hybridization (DOH) of the fuel cell vehicle, which represents the division between fuel cell and battery power. This is an important concept in the initial sizing of component for a fuel cell vehicle to best reduce fuel consumption and battery strain.

Moving to offline approaches which allow global optimality to be determined, Wang *et al.* [9] explored specific problems associated with applying DP to the energy management of a plug-in diesel-electric hybrid bus, simplifying the continuous problem to a discretized model and adjusting the resolution of discretization of the variables. The study evaluated the selection of a proper resolution for DP to have a reasonable computational load while still obtaining a close-to-optimal power management solution. Ultimately, achieving a balance of adequate resolution without excessive computational requirement in the DP can lead to valuable insight for an online optimization. O'Keefe and Markel [10] used a DP approach to evaluate energy consumption of a Plug-in Hybrid Electric Vehicle (PHEV). Taking the results of the DP into consideration, the conclusions were that driving the PHEV in urban environments is better in an "electric vehicle centric mode" rather than a "blended mode", using more electric stored energy earlier on in a typical drive rather than beginning in a fully blended mode between gas engine and electric motor.

Marx [11] applied multiple optimization techniques for comparison to a rule-based controller of a fuel cell-battery-supercapacitor powertrain. One key finding among all the techniques was how the instantaneous optimality control strategy resulted in a cost performance within 3% of the DP, when the PI rule-based controller was more than 30% greater cost than DP. This shows the great potential for an instantaneous optimality controller as a real-time controller over a simple rule-based controller.

Transitioning to studies which focus more on the connected and automated vehicles, Malikopoulos, Cassandras, and Zhang [12] developed a decentralized optimal control framework whose closed-form solution exists under certain conditions, and which, based on Hamiltonian analysis, yields for each connected vehicle the optimal acceleration/deceleration at any time in the sense of minimizing fuel consumption. The solution allows the vehicles to cross an intersection without the use of traffic lights, without creating congestion, and under the hard safety constraint of collision avoidance.

Kang *et al.* [13] built a queue length model to estimate the number of vehicles waiting at a traffic light to accurately optimize the velocity profile for pure electric vehicles. To predict the arrival rate at each intersection, a deep learning Stacked autoencoders (SAE) model was used. Ichikawa *et al.* [14] utilized GPS navigation in combination with driving data, to update the controls of a hybrid energy management system (EMS). This solution can be thought of as a quasi-DP approach with a limited amount of previous data storage to update the powertrain controls periodically. Hu *et al.* [15] considered a car following model with both V2V and V2I communication. Sequential quadratic programming was used to determine the optimal velocity of the following vehicle, and a simulation performed to compare results with and without connectivity. Maximum size of the prediction control horizon used in the quadratic programming was determined to have a maximum of 1 second compute time with a 1.4 GHz CPU, for online use.

As the current paper investigates the impact of connectivity on battery degradation, a study which used experimental results to form an empirical relationship for $LiFePO_4$ cell degradation was chosen. Wang *et al.* [16] developed a comprehensive degradation model for commercially available 26650 cylindrical cells made by A123 Systems which was tested at different discharge rates (C-rates). The empirical formula was developed based on the C-rate, Amp-Hour throughput, and temperature. This degradation formula is useful for estimating potential increases in battery lifetime with V2I implementation.

The research reviewed above represents a comprehensive study of optimal control methods for a variety of different vehicles and scenarios. One aspect which does not appear to be covered to date is quantifying the extent to which V2I implementation can reduce the overall cost when both energy consumption and battery degradation are included in the optimization. To our knowledge, none of these listed studies nor others in literature have used connectivity in combination with energy consumption and battery life. Our work focuses on one idealized intersection to understand the impact of connectivity on the speed profiles, and consequently on energy consumption and battery degradation. We assumed a model layout to demonstrate our methodology which can be extended in the future to more realistic traffic layout scenarios. Furthermore, considering the tradeoffs between different battery sizes when implementing connectivity is a new area of exploration. The results obtained herein may help to determine the optimal battery size for an electric bus given a real-world driving scenario, as well as determining the payback of implementing V2I technology in city environments.

The structure of the paper is as follows. In Section II we formulate the problem and present the modeling framework. In Section III, we provide the DP formulation, and in Section IV we show how DP is implemented. Finally, we provide simulation results in Section V and concluding remarks in Section VI.

II. Problem Formulation

An electric bus (EB) traveling through a single intersection is modeled in this study. Dynamic programming is applied to find the optimal velocity profile (considering both energy consumption and battery degradation) and the resulting overall cost benefits of having connectivity compared to the baseline case with no connectivity.

A single intersection is utilized where the control zone extends from 200 m prior to and 200 m past the intersection. These distances were chosen based on an average block length typical of less densely populated U.S. cities [17]. The EB enters the control zone at 35 mph and is required to attain the speed of 35 mph as it exits the control zone. The top speed of 35 mph was estimated from the average cruising speed for a typical city bus [18].

The intersection has a timed light sequence which consists of 60 seconds green, followed by 4.5 seconds yellow and 30 seconds red. The light timing was chosen based on an average urban cycle length for major and minor throughways by the National Association of City Transportation Officials [19]. Other timing sequences and control zone distances could be applied using the methodology in this study. Each simulation is characterized based on the timing of the bus as it enters the control zone. To cover all possible signal timing cycles of the unconnected baseline cases and connected cases, multiple optimum velocity profile simulations were run for each cycle with one second separation between different cycles. The first situation considered was the light turning green immediately upon vehicle entry into the control zone. A complete series of light changes was considered to ensure that all scenarios were simulated. A simple rule-based controller subjected to velocity and acceleration constraints was used for the unconnected baseline cases.

A. Electric Bus (EB) Powertrain

A simplified EB model was considered, in which the energy required by the traction motor (TM) as well as the battery size was included. The effect of three different bus masses and three different battery sizes was investigated. The technical parameters of the EB are summarized in Table I.

B. Vehicle Model

A simplified vehicle model is used. The forces acting in the longitudinal direction include the rolling resistance of the front and rear tires (F_{roll}), aerodynamic drag (F_{aero}), acceleration resistance (F_{accel}), and traction force on the drive wheels (F_{drivew}). For the simulation, the grade is assumed to be equal to zero. The dynamic equation for the vehicle along the longitudinal direction is given by [8],

$$\begin{aligned} F_{\text{drivew}} &= F_{\text{roll}} + F_{\text{aero}} + F_{\text{accel}} \\ &= mgf + 0.5\, C_D \rho\, Av^2 + m\frac{dv}{dt} \end{aligned} \tag{1}$$

where m is the vehicle gross weight, g is the acceleration due to gravity, f is the rolling resistance coefficient, C_D is the aerodynamic drag coefficient, A is the vehicle frontal area specified in Table I, ρ is the air density, v is the vehicle velocity, and $\frac{dv}{dt}$ is the vehicle acceleration. Acceleration is described as a function of the current velocity and desired velocity at the next time step, t_{step}:

$$a_k = \frac{v_{k+1} - v_k}{t_{\text{step}}} \tag{2}$$

Finally, the torque required is

$$T_{req,k} = \frac{r_d}{i_0 \eta_T}\left[mgf + 0.5\, C_D \rho A v^2 + m a_k\right] \tag{3}$$

where r_d is the dynamic radius of the wheel, i_0 is the fixed transmission gear ratio, and η_T is the transmission efficiency listed in Table I.

TABLE I
Electric Bus Model Parameters

Powertrain	Parameter	Value	Parameter	Value
Traction Motor	Max Power (kW)	180	Max Torque (Nm)	833.5
	Max Regenerative Power (kW)	110	Max Regenerative Torque (Nm)	706.4
Others	Gross	12,100/	Aerodynamic	0.80
	Weight (kg)	12,950 / 13,800	Drag (Cd)	
	Frontal Area (m^2)	4.81	Rolling Resistance Coefficient	0.0065
	Tire Rolling Radius (m)	0.369 @20m/s	Transmission Efficiency	0.8536
	Battery Size	81 kWh / 162 kWh / 324 kWh	Fixed Transmission Gear Ratio	10.26: 1

C. Traction Motor Model

Since the actual vehicle motor model is unavailable, the motor efficiency model in [20] is employed. These efficiency values were extracted into a discrete table and utilized for both the positive regions of torque demand, as well as the negative regenerative braking regions of torque demand. The required torque from equation 3 is modified by the motor efficiency to obtain net energy per step.

D. Battery Degradation Model

A battery aging model from [21] is used in which the battery's end-of-life is defined as when the current battery capacity reaches 80% of its original capacity. The following semi-empirical model is used to calculate degradation:

$$\Delta Q_b = M(c) \exp\left(\frac{-E_a(c)}{RT_c}\right) A(c)^z \tag{4}$$

where ΔQ_b is the capacity loss in percent, c is C-rate, $M(c)$ is the pre-exponential factor as a function of C-rate (see Table II below), R is the ideal gas constant, T is the temperature (set to 294 K), and A is the amp-hour throughput which depends on the

TABLE II
$M(c)$ PRE-EXPONENTIAL FACTORS FOR C-RATE [15]

C-rate	0.5	2	6	10
M(Pre-factor)	31630	21681	12934	15512

C-rate. The exponent z is a constant and equal to 0.55, and E_a is the activation energy, given by:

$$E_a\left(c\right) = 31700 - 370.3c \tag{5}$$

By calculating the total amp hour throughput and differentiating the state of health (SOH) equation (not shown here), [21] shows how equations (4) and (5) are used to derive (6) below. Thus, the instantaneous change in the battery's SOH, i.e., battery degradation, is determined as follows:

$$\frac{dSOH}{dt}\left(t\right) = -\frac{\left|I\left(t\right)\right|}{2N\left(c, T_c\right) C_{\text{bat}}} \tag{6}$$

where $I(t)$ is the current at the instantaneous step, N is the equivalent number of battery cycles from 0 SOC to full capacity, and C_{bat} is the nominal capacity of the battery. The units of $\frac{dSOH}{dt}$ are 1/s. The degradation incurred during a given time step is obtained by multiplying the instantaneous degradation rate by the corresponding time step.

For practical purposes, public transit vehicles must have a certain minimum battery size to accommodate sufficient transit miles. Three battery configurations are studied here: the largest is a 324 kWh battery, based on the popular BYD K9 bus. In addition, a half-size battery of 162 kWh as well as a quarter-size battery of 81 kWh are also studied to evaluate the influence of battery size. It is important to note that according to [16], which detailed $LiFePO_4$ cell degradation, the depth-of-discharge for low C-rates ($c < 1$) has minimal impact on degradation. According to the manufacturer's specifications, the maximum possible C-rate the quarter-size battery with 11,157 cells experiences is 0.98C while using 180kW max motor power. Therefore, the effect of depth-of-discharge is neglected in this study based on the findings of [16] with C-rate being less than 1C. Moreover, the charge/discharge efficiency at low C-rates is very high and is set to 1. This high round- trip efficiency is confirmed by a voltage discharge vs. capacity chart provided by the manufacturer for different C-rates [22].

III. DYNAMIC PROGRAMMING FORMULATION

The optimal control problem is formulated below and solved by a deterministic DP algorithm as it guarantees global optimality and serves as a benchmark. DP is generally computationally intensive and may not be suitable for real-time application, but this will not pose a problem for our study since optimal velocity profiles can be generated offline. These velocity profiles can be subsequently implemented into a real-time controller using a lookup table for varying distance and signal timing scenarios. The following variables are used for the state and action space, and cost function:

State space (x_k): vehicle speed (v)

Action space (u_k): motor torque ($T_{req,k}$) with dynamic equation of the system:

$$x_{k+1} = f\left(x_k\ ,\ u_k\right) \tag{7}$$

Cost Function (G): The cost function consists of the electric energy consumption and battery degradation, which is a function of motor torque ($T_{req,k}$), motor speed (RPM), and motor efficiency

$$J = \sum_{k=0}^{N-1} G\left(x_k, u_k\right) \tag{8}$$

where N is total number of road segments, and k is the index of road segments. To provide additional details of the cost function, the following equation shows how the energy consumption and battery degradation are combined to obtain the overall cost:

$$G\left(x_k, u_k uk\right) = x_k\ C_e\ T\omega dt/\eta + C_b\dot{Q}dt \tag{9}$$

where C_e is the electricity cost, T is the motor torque, ω is the motor speed in radians per second, dt is the time step, η is the motor efficiency, C_b is the battery cost and $\dot{Q}$ is the battery degradation rate. Note that we are only optimizing the pre-intersection portion of the vehicle's velocity profile; we assume that the velocity profile after the intersection is the same for the connected and non-connected cases. Signal timing at the intersection is introduced by bounding the total travel time to reach the intersection. The DP algorithm can fall into unreachable states if the bounding time is too tight because the algorithm is unable to choose a velocity trajectory which falls within the specified cycle time. Therefore, a small time-buffer (0.2 seconds) is provided both before and after the precise travel time to prevent such unreachable states.

To correctly implement the DP formulation, many constraints must be imposed. First, there are the upper and lower bounds for the state variables of velocity and acceleration:

$$\begin{cases} 0 \le v\left(t\right) \le v_m \\ a_m \le a\left(t\right) \le a_M \end{cases} 0 \le t \le T \tag{10}$$

where v_m denotes the maximum speed (35 mph), a_m and a_M denote the maximum deceleration and acceleration respectively, which are determined by the maximum motor torque at the corresponding motor RPM.

The overall minimization problem is formulated as follows

$$\min J = \sum_{k=0}^{N-1} G\left(x_k, u_k\right) \tag{11}$$

subject to:

$$t_f = T_{ttg}\ \pm T_{\text{buffer}} \tag{12}$$

$$v_0 = 35 \tag{13}$$

$$u_k = T_{TM} \tag{14}$$

Equation (12) is a travel time constraint where T_{ttg} is time-to-green light and T_{buffer} is the allowed buffer in total travel time.

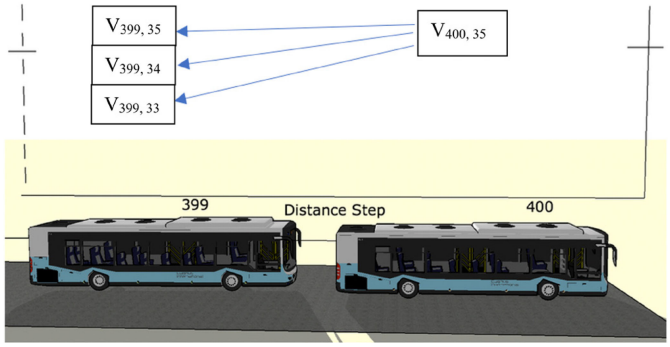

Fig. 1. An example of solving for the optimal velocity trajectory using the DP algorithm. The velocity index values for the last position step (at 400 m) to the second-to-last index step (at 399 m) are shown. The velocity indices are shown by 35, 34, 33 mph on the left.

Equation (13) defines the initial state by hard setting the initial entry speed to the control zone at 35 mph. For the control input constraint (14), torque required is equal to the traction motor torque. Note that no air brake torque is considered in this study because the traction motor can apply the required braking force.

Based on Bellman's equation [23], DP solves the following equation recursively:

$$J_k^*(x_k) = min_{u_k}\left[G(x_k, u_k) + J_{k+1}^*(x_{k+1})\right] \tag{15}$$

where $J_k^*(x_k)$ is the cost-to-go function at state x_k. The cost-to-go is defined as the total cost from the current position until the end of the control zone. This minimum function in (15) searches for and finds the optimal control input and yields the optimum velocity profile for the bus under connected vehicle scenarios. For the non-connected scenarios, a predetermined velocity profile is assigned based on the way a human driver would control the vehicle while viewing the traffic light ahead. This predetermined velocity profile is discussed in the results section.

In this study, the maximum motor torque corresponding to 13 discrete motor speed values is stored for calculation of the constraints. The value of motor efficiency is interpolated at the corresponding velocity and motor torque.

IV. Dynamic Programming Implementation

A. Dynamic Programming Implementation

The distance to the intersection is discretized to solve by the DP algorithm. The spacing between each distance node is chosen as 1m. The time step, t_{step} is calculated for each segment based on velocities between adjacent nodes. The analysis is carried out in two parts: pre-intersection and post-intersection. The post-intersection recursive dynamic programming is done first to set the cost-to-go to zero for the exit velocity of the control zone. At each of the previous velocity indices, the energy and battery degradation cost-to-go are summed, and the minimum combined cost is assigned as the cost-to-go value for each velocity index. This process is depicted in Fig. 1. The velocity indices (shown by 33, 34, 35 mph) are discretized with far higher resolution (0.01 mph) than shown in the figure for accurate results. That index is then selected, and the process repeats for the previous position step (398 m), working backwards until a complete velocity trajectory is determined for the post-intersection. For the pre-intersection, all possible cost-to-go values for each velocity index at the intersection are first calculated based on the cost-to-go results of post-intersection calculations. Then the minimum cost assigned to each velocity index at its respective position index is calculated recursively from end to start of the pre-intersection, using only feasible states. An important note is that there is no weighting applied between energy cost and battery degradation cost, rather the absolute cost of each is summed. In addition, a constant acceleration was forced upon entry to the post-intersection to maximize traffic throughput by preventing unnecessary delays. The average simulation time using Matlab to process the pre-intersection DP was approximately 90 minutes depending on the light cycle timing, using a PC with an average speed 4-core processor.

B. Light Cycle Timing Implementation

For the timing of the lights, a two-element array is initialized. The first element represents the time in seconds to red upon entering the control zone, and the second element represents time in seconds to the next green. For example, [0 8] represents the traffic light being red upon entry to control zone and turning green 8 seconds from the time of entry. In another example, [1 31] signifies that the light is currently green upon entry into the control zone and will turn red in 1 second. The time to the next green is 31 seconds.

V. Simulation and Results

A. Overview of Non-Connected and Connected Vehicle Velocity Trajectories

Three distinct situations can occur as the bus transits the control zone. The first is when the vehicle can maintain maximum speed throughout the entire control zone. This is the simplest case, and the total energy required is determined by summing costs at each step while traveling at 35 mph. This case occurs for the non-connected scenarios when the light is red upon vehicle entry and turns green in less than or equal to 9.6 seconds after entry. However, only round number cycle times are used, so the [0 9] timing sequence is the break-point for the first situation. Over 9 seconds at 35 mph, the bus would travel 141m into the control zone, which is still less than the prescribed distance of 150 m at which point the driver would apply the brakes if the light were still red. For the connected case however, maximum speed can be maintained throughout the control zone when the light is red upon entry and turns green in less than or equal to 12.8 seconds. Thus, the connected vehicle can maintain maximum speed for 3 additional seconds (using a round number cycle time of 12 seconds) because it does not need to brake as the cycle timing is known a priori. Additionally, for both connected and non-connected scenarios, maximum velocity throughout the control zone can be maintained when the light is green upon entry and turns red in 12.8 or more seconds. The reason the maximum velocity can be maintained in the non-connected

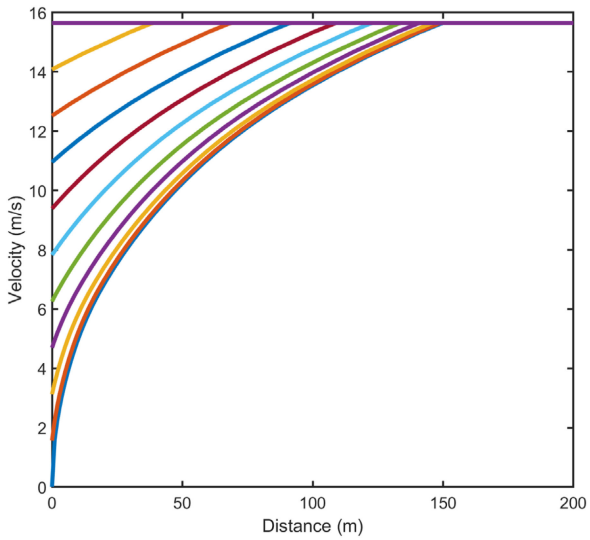

Fig. 2. Selected post-intersection velocity trajectories for the full-size configuration. Each curve is a distinct velocity trajectory based on the entry velocity into the post-intersection (shown in 1.56 m/s increments). Both connected and non-connected cases have identical post-intersection trajectories.

vehicle for this situation is that even though the light turns yellow at 8.3 seconds into the control zone (at the 130 m mark) and the driver is able to see it before reaching a safe stopping distance (150 m), the driver is assumed to be familiar with the cycle timing and knows that the light can be cleared safely before it turns red without accelerating beyond 35 mph.

The second case is when the vehicle must come to a complete stop. This occurs for the non-connected scenarios when the light is red upon entry to the control zone, and there are 16 or more seconds to green (as it takes 15.9 s to reach the intersection while traveling at maximum velocity to the 150 m mark, and then braking all the way from 150m to 200 m; again only round number cycle times are considered). The complete stop case also occurs if the vehicle enters during a green and there are 12.8 s or less to red; then, it would have to make a complete stop to avoid running through a red light. For the connected scenario, the vehicle need not to come to a complete stop for any cycle time as this is not optimal.

For the third case, the vehicle enters the control zone while the light is red and turns green while the vehicle is somewhere between 150 m and 200 m. For the non-connected case, the driver begins to brake at the 150 m mark, and upon seeing a green light, accelerates back up to speed. This happens in six distinct cycle timing scenarios when the time-to-green is 10 to 15 s after the vehicle enters the control zone. These situations do not occur in the connected scenarios, as the vehicle can slow down a small amount at an earlier position to achieve the optimal velocity trajectory.

B. Post-Intersection Velocity Trajectory Results

For both the connected and non-connected cases, the same velocity trajectories after the intersection are used. Fig. 2 shows the prescribed velocity trajectory after the intersection based on the velocity immediately past the intersection. Note that only selected post-intersection trajectories (incremented by 1.56 m/s or 3.5 mph) are shown for clarity; however, a full set of finely discretized velocities is executed in the simulation and stored to calculate the final combined cost of energy consumption and battery degradation in the DP of the pre-intersection. Separate simulations are run to calculate the total energy consumption cost and the battery degradation cost for the post intersection.

C. Pre-Intersection Results

Optimization is beneficial only for the pre-intersection, where it is applied. To highlight the difference between non-connected and connected cases, two cycle timings are shown: [0 14] and [11 41]. Results are presented for the full-size and quarter-size battery vehicle configurations. For the [0 14] timing cycle shown in Fig. 3(a), the non-connected vehicle trajectories for both battery configurations are identical. The driver maintains the top speed of 35mph until 150m at which point the brakes are applied. Upon seeing the green light at 14 seconds (193 m) after entering the control zone, the driver then accelerates toward the intersection (note that human reaction time is neglected here). In the connected case for the [0 14] cycle time, both battery configuration vehicles follow virtually identical velocity trajectories. They both decelerate initially for the first 20 m and then maintain a speed of about 14 m/s to the intersection. The overall cost reduction (in energy consumption and battery life) for this cycle timing in going from non-connected to connected is 65% and 62%, respectively, for the full-size and quarter-size configurations. The large reduction in cost is primarily because the connected vehicle does not need to brake and reaccelerate as severely as the non-connected vehicle. The full-size battery configuration returns a slightly bigger cost saving owing to its greater vehicle mass, i.e., net amp-hour throughput. The C-rate in this case has a negligible effect on both configurations.

For the [11 41] cycle time shown in Fig. 3(b), the non-connected trajectories for the full-size and quarter-size battery are again identical. Both vehicles must now come to a complete stop because the driver does not know the light timing a priori. However, it is most optimal for the bus to not stop, which can be achieved for the connected cases. As shown in Fig. 3(b), the connected full-size battery bus decelerates for the first 85 m and then maintains a slow speed of about 4 m/s to the intersection, whereas the connected quarter-size battery bus decelerates for the first 75 m and maintains a similar speed of approximately 4 m/s to the intersection. The full-size battery vehicle, being heavier, decelerates more slowly to maintain higher motor efficiency throughout the regenerative braking process. A second, smaller, factor is air drag. Attaining a lower speed as soon as possible to minimize air drag is optimal, but this is countered by poor motor efficiency if the vehicle decelerates too quickly. A breakdown of the power losses contributed by these various mechanisms is shown in Fig. 4 and will be discussed in detail subsequently. By remaining in motion, the total cost for the [11 41] cycle time is reduced in going from non-connected to connected by 36% and 50%, respectively, for the full-size and quarter-size battery configurations. For the full-size battery, energy cost is reduced

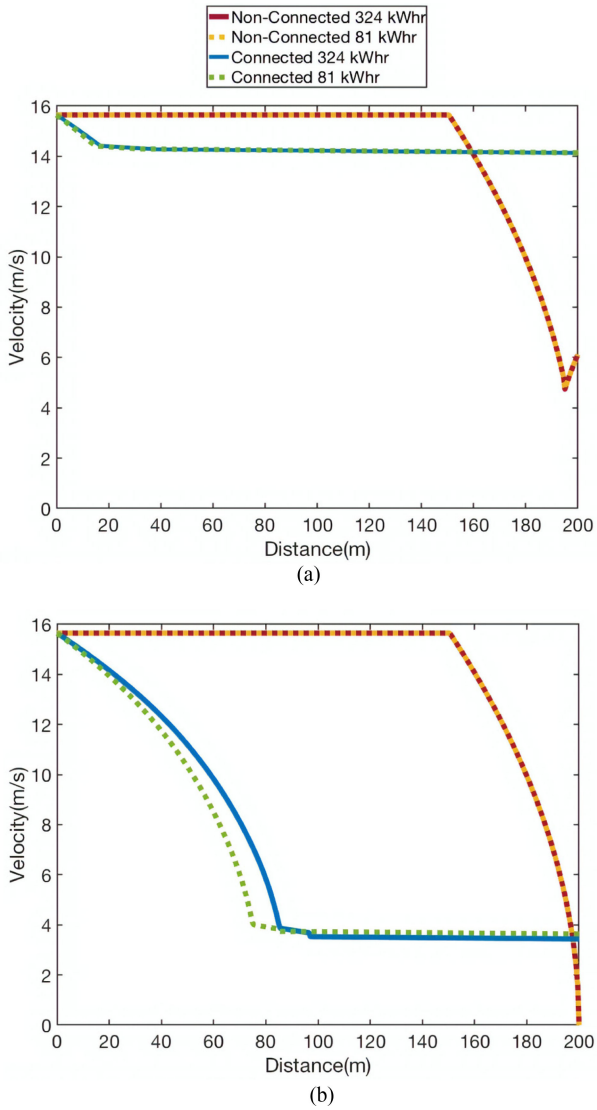

Fig. 3. Pre-intersection velocity trajectories for the full-size (324 kWh) and quarter-size (81 kWh) battery configurations. (a) [0 14] cycle time, and (b) [11 41] cycle time. For the non-connected cases, both battery configurations show the identical velocity trajectory.

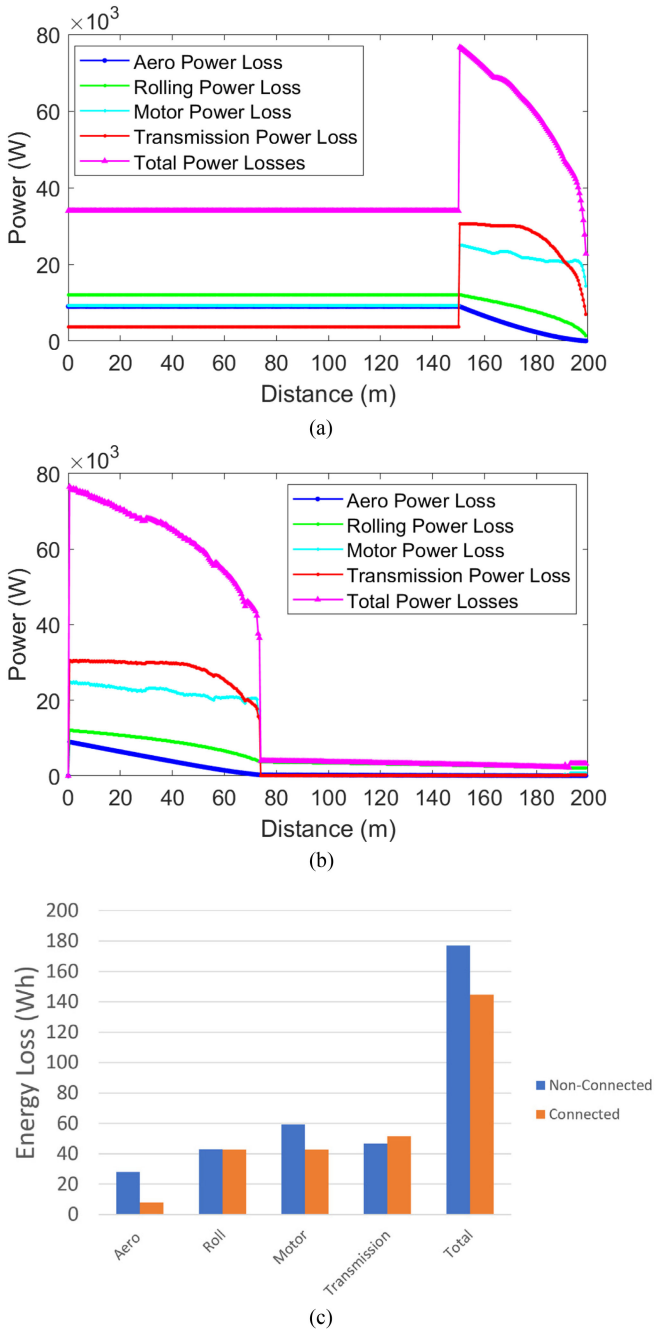

Fig. 4. Power loss contributors for the quarter-size 81 kWhr battery, [11 41] cycle time, pre-intersection region. (a) Non-connected case; (b) connected case; (c) comparison of energy losses for each contributor.

by 33% and battery degradation cost is reduced by 3%. However, for the quarter-size battery, energy cost is also reduced by 33% but battery degradation cost is reduced by 17%. This is due to the high C-rate for the non-connected quarter-size configuration. With fewer cells available to distribute the load, the quarter-size battery configuration experiences high degradation during hard-braking situations which is mitigated for the connected case.

The breakdown of the power losses contributed by air drag, rolling resistance, and motor and transmission inefficiencies are compared between the non-connected and connected cases in Fig. 4(a) and (b), respectively, for the quarter-size 81 kWhr battery and [11 41] cycle time. Fig. 4(c) shows that connectivity results in a 71% reduction in air drag energy loss due to an earlier slowdown in the pre-intersection. Energy loss from rolling should be exactly the same in both scenarios because it is equal to the rolling resistance (mgf) times the distance traveled. Fig. 4(c) reveals that the energy loss due to rolling resistance for the two cases agrees to within 0.25% due to the high fidelity of the simulation. Motor energy loss is determined by the motor efficiency at each respective torque and motor rpm value for a given velocity trajectory; in this specific example, motor energy loss drops by 28% for the connected case. The 10% increase in transmission energy loss in going from non-connected to connected is counterintuitive and can be explained as follows. In the connected case, the vehicle follows a more efficient velocity profile within the pre-intersection which allows more

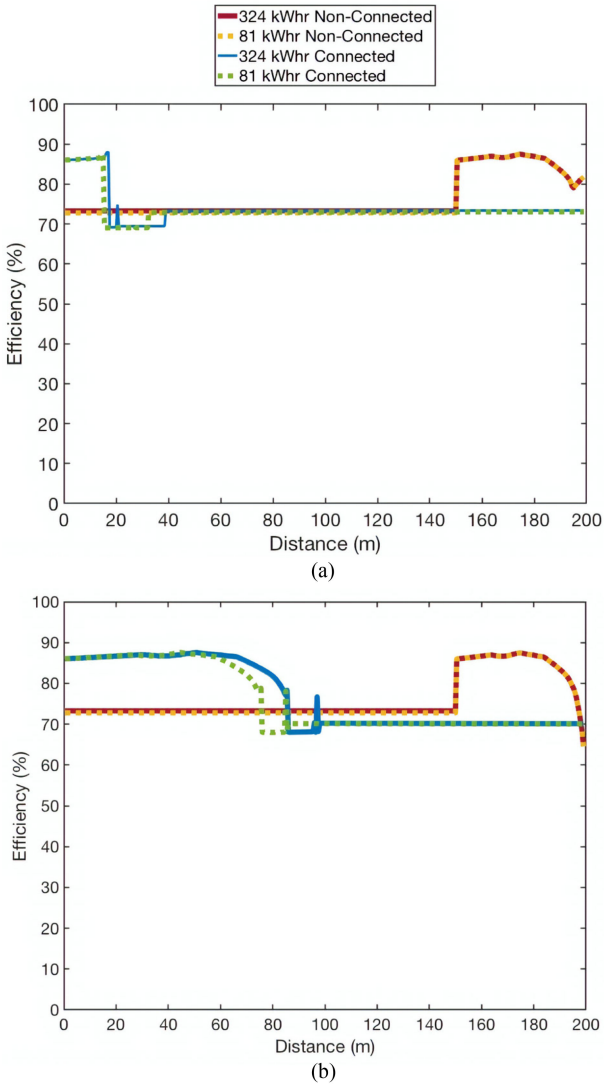

Fig. 5. Motor efficiency trajectories for the full-size (324 kWh) and quarter-size (81 kWh) battery configurations. (a) [0 14] cycle time, and (b) [11 41] cycle time.

energy to be captured through regenerative braking. Because this greater energy must travel through the transmission to reach the batteries, the bus incurs a higher transmission loss. Overall, it is still more efficient for the bus to gently brake upon entering the pre-intersection under a connected scenario such that a net 18% reduction in energy losses is observed for the pre-intersection portion. It is important to note that the 33% energy cost reduction mentioned previously pertained to the entire intersection.

The motor efficiency trajectories are shown in Fig. 5 for each timing cycle. Motor efficiency trajectories are nearly identical for the [0 14] non-connected configurations (Fig. 4(a)) since their velocity trajectories are identical. The motor efficiency is seen to be around 72% till the 150m mark, and then rises to about 88% when the driver applies the brakes. The motor efficiency rises sharply during deceleration because the motor is more efficient for mid-range values of torque and rpm. Likewise, the motor efficiency trajectories for the connected [0 14] cases in Fig. 5(a) are similar due to their nearly identical velocity trajectories. Both configuration trajectories start high at about 87% for the first 18m and then drop to a lower level for the remainder of the pre-intersection for the same reason (the motor is more efficient for the torque and combination during the deceleration phase). The motor efficiency stays at around 72% for all four cases between 40 and 200 m, as this is the highest possible efficiency for the corresponding velocity trajectories. For the [11 41] non-connected cases shown in Fig. 5(b), a similar motor efficiency profile is again seen due to their identical velocity trajectories. For the [11 41] connected cases, the motor efficiency of the quarter-size battery vehicle drops sooner than the full-size battery vehicle because the quarter-size battery vehicle reaches the 4 m/s cruising speed earlier. The motor efficiency drops to about 70% for both vehicles as they travel through the remainder of the pre-intersection at 4 m/s because the motor is less efficient at mid-torque and low rpm values.

The battery degradation trajectories are shown in Fig. 5 for each timing cycle. A general observation in Fig. 5(a) and (b) is that the battery degradation rate is much higher for the smaller battery in both non-connected and connected cases due to its expectedly higher C-rate. For the non-connected cases, the degradation rate is small for the first 150 m when the vehicle is cruising at constant speed because the only power demand on the battery comes from overcoming air drag which is small. Beyond 150 m, the battery degradation increases when the battery experiences a surge of regenerative current during deceleration. The degradation increases from 150 to 180 m for the quarter-size battery non-connected vehicle because of several factors. The air-drag decreases as the vehicle slows from 15.6 to about 10m/s, while the motor efficiency increases. These factors cause the battery to accept more regenerative current. At 180 m, the quarter-size battery degradation begins to decrease because the motor efficiency decreases (see Fig. 5(a) and (b)). A lower motor efficiency implies that more of the vehicle's kinetic energy is lost to heat due to motor electric losses with a correspondingly smaller braking load on the battery. The influence of motor efficiency and air drag on battery degradation is further confirmed when comparing the last 7m of vehicle travel for the quarter-size battery vehicle in Fig. 6(a) and 6. In the [0 14] cycle, quarter-size degradation drops to about 1.4E-9/s. But for the [11 41] case, the quarter-size degradation drops to only about 1.2E-9/s because the motor is less efficient in the [11 41] cycle (Fig. 4(b)) than the [0 14] cycle (Fig. 5(a)). One other note is the small spikes which can be seen in Fig. 5(b) at 85 m and 95 m, and the pronounced spike in Fig. 6(b) at 85 m. These spikes are due to discretization and were reduced to the minimal possible level; further reduction would have entailed prohibitively long computational times.

D. Cost Comparisons

To compare between non-connected and connected cost, an equally weighted average was taken from all the 60 possible timing cycles. Energy consumption cost and battery degradation cost were tracked separately during simulation and are shown in Fig. 7. The cost for electricity usage was based on the U.S. Energy Information Administration's 2018 average

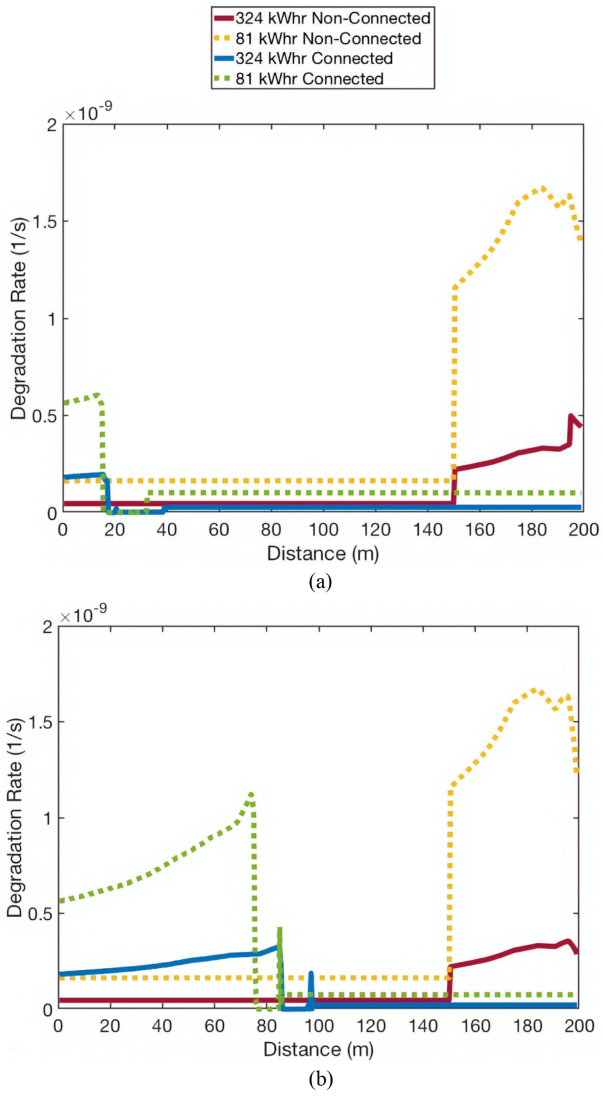

Fig. 6. Battery degradation trajectories for the full-size (324 kWh) and quarter-size (81 kWh) battery configurations. (a) [0 14] cycle time, and (b) [11 41] cycle time.

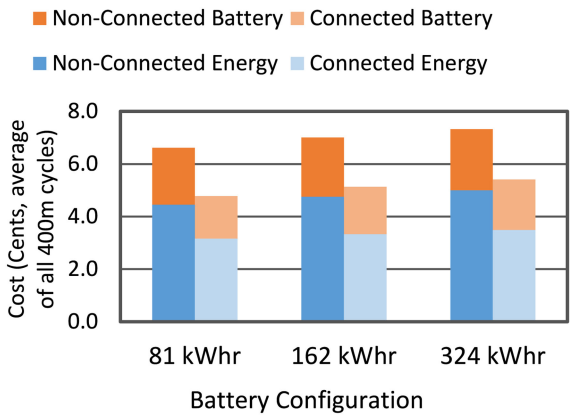

Fig. 7. Overall energy and battery degradation cost averaged over all timing cycles for a single pass through the 400m control zone for the three battery configurations for the connected and non-connected cases.

transportation electricity cost of 9.8 cents/kWh [24]. The cost for the battery was based on Bloomberg's average Battery Electric Vehicle (BEV) transportation-specific cost of $150/kWh [25]. The reduction of cost in going from the non-connected to connected case is immediately apparent. The average cost reduction for all three configurations is 27% when connectivity is applied. The biggest contributor to cost savings comes from the mid-timing cycles (from [0 12] to [12 42]) as illustrated in Fig. 3. The greatest cost reduction is seen in the quarter-size battery vehicle (27.5%), while the least cost reduction is seen in the full-size battery vehicle (25.8%). This is due to the high C-rate for non-connected cases in the quarter-size configuration, which is alleviated when connectivity is employed. The full-size battery vehicle does not experience as high a degradation cost for the non-connected cases due to having so many cells to reduce the average C-rate.

For the battery degradation cost, the results may not be intuitively obvious. There is greater degradation associated with the largest battery than the smallest in both non-connected and connected cases. This is because there are the two balancing factors of having more mass which increases degradation, and fewer cells, which also increases degradation. At some point, for battery sizes even smaller than those employed in this study, the C-Rate will become the dominant factor and total cost will be more than in larger battery size configurations due to this high degradation cost.

VI. Conclusion

An optimal power management system was studied for an electric bus traveling through a signalized intersection and it was determined that an average of 27% reduction in cost may be realized by employing connectivity to obtain a prior knowledge of the traffic-light cycle timing. The cost was broken down in terms of energy consumption cost and battery degradation cost for three different battery sizes. The amount of cost reduction depends on the cycle lengths, battery size, vehicle mass, and distances used in the control zone leading up to and following the intersection. The smallest size battery experienced the greatest saving when employing connectivity compared to the baseline case. Future studies may improve upon this model by adding more complex control zones and implementing different timing cycles. Alternate battery degradation models for various other chemistries can be easily studied using the current framework.

References

[1] Q. LiHong, Q. LiJun, Z. Hesam, and P. Pierluigi, "Design and optimization of equivalent consumption minimization strategy for 4WD hybrid electric vehicles incorporating vehicle connectivity," *Sci. China*, vol. 61, no. 1:147–157, Jan. 2018.

[2] J. Liu and H. Peng, "Modeling and control of a power-split hybrid vehicle," *IEEE Trans. Control Syst. Technol.*, vol. 16, no. 6, Nov. 2008.

[3] J. Han and Y. Park, "A novel updating method of equivalent factor in ECMS for prolonging the lifetime of battery in fuel cell hybrid electric vehicle," *Int. Federation Autom. Control*, pp. 227–232, Oct., 2012.

[4] C. Lin, H. Peng, and J. Grizzle, "A stochastic control strategy for hybrid electric vehicles," in *Proc. Amer. Control Conf.*, Jun./Jul. 2004, pp. 4710–4715.

[5] C. Vagg, S. Akehurst, C. Brace, and L. Ash, "Stochastic dynamic programming in the real-world control of hybrid electric vehicles," *IEEE Trans. Control Syst. Technol.*, vol. 24, no. 3, pp. 853–866, May 2016.

[6] A. A. Malikopoulos, "Stochastic optimal control for series hybrid electric vehicles," in *Proc. Amer. Control Conf.*, Jun. 2013, pp. 1189–1194.

[7] A. A. Malikopoulos, "A multiobjective optimization framework for online stochastic optimal control in hybrid electric vehicles," *IEEE Trans. Control Syst. Tech*, vol. 24, no. 2, pp. 440–450, Mar. 2016.

[8] M. Kim and H. Peng, "Power management and design optimization of fuel cell/battery hybrid vehicles," *J. Power Sour.*, vol. 165, no. 2, Mar. 2007, pp. 819–832.

[9] X. Wang, H. He, F. Sun, and J. Zhang, "Application study on the dynamic programming algorithm for energy management of plug-in hybrid electric vehicles," *Energies*, vol. 8, pp. 3225–3244, Apr. 2015.

[10] M. O'Keefe and T. Markel, "Dynamic programming applied to investigate energy management strategies for a plug-in HEV," in *Proc. NREL/CP-540-40376 Conf. Paper*, 22nd International Battery, Hybrid and Fuel Cell Electric Vehicle Symposium and Exhibition (EVS-22), Nov. 2006, pp. 1–12.

[11] M. Marx, "Multiobjective optimization of the power flow control of hybrid electric power train systems with simulated and experimental emulation applications," in *Proc.* Retrieved from Universitat Duisburg-Essen, Ph.D. Thesis, 2014. [Online]. Available: https://d-nb.info/1050933346/34

[12] A. A. Malikopoulos, C. Cassandras, and Y. Zhang, "A decentralized energy-optimal control framework for connected automated vehicles at signal-free intersections," *Automatica*, vol. 93, no. 7, pp. 244–256, 2018.

[13] L. Kang, H. Shen, and A. Sarker, "Velocity optimization of pure electric vehicles with traffic dynamics consideration," in *Proc. IEEE 37th Int. Conf. Distrib. Comput. Syst.*, Atlanta, GA, 2017, pp. 2206–2211.

[14] S. Ichikawa *et al.*, "Novel energy management system for hybrid electric vehicles utilizing car navigation over a commuting route," *IEEE Intell. Veh. Symp.*, pp. 161–166, 2004.

[15] X. Hu, H. Wang, and X. Tang, "Cyber-physical control for energy-saving vehicle following with connectivity," *IEEE Trans. Ind. Electron*, vol. 64, no. 11, pp. 8578–8587, Nov. 2017.

[16] J. Wang *et al.*, "Cycle-life model for graphite-LiFePO$_4$ cells," *J. Power Sources*, vol. 196, pp. 3942–3948, Dec. 2010.

[17] A. Price, "Optimizing the street grid," 2013. [Online]. Available: https://www.strongtowns.org/journal/2013/11/27/optimizing-the-street-grid.html, Accessed on: Apr. 20, 2019.

[18] D. Hertz, "Urban buses are slowing down," 2015. [Online]. Available: http://cityobservatory.org/urban-buses-are-slowing-down/, Accessed on: Apr. 20, 2019.

[19] "Urban street design guide," 2019. [Online]. Available: https://nacto.org/publication/urban-street-design-guide/intersection-design-elements/traffic-signals/signal-cycle-lengths/, Accessed on: May 2, 2019.

[20] Miroslav Chomat. *New Applications of Electric Drives*. Intech Open Access. Dec. 2015.

[21] H. Perez *et al.*, "Optimal charging of li-ion batteries with coupled electro-thermal-aging dynamics," *IEEE Trans. Veh. Technol.*, vol. 66, no. 9, Sep. 2017.

[22] A123 Systems, "Nanophosphate high power lithium ion cell ANR26650M1-B," *Manufacturer Specification Sheet*, 2012. [Online]. Available: https://www.batteryspace.com/prod-specs/6610.pdf

[23] P. Kumar and P. Varaiya, in *Stochastic Systems: Estimation, Identification, and Adaptive Control*. Englewood Cliffs, NJ. Prentice Hall, Inc. 1986.

[24] "Electric power monthly," U.S. Energy Information Administration. 2019. [Online]. Available: https://www.eia.gov/electricity/monthly/epm_table_grapher.php?t=epmt_5_6_a, Accessed on: May 2, 2019.

[25] C. Curry, "Lithium-ion battery costs and market," 2017. [Online]. Available: https://data.bloomberglp.com/bnef/sites/14/2017/07/BNEF-Lithium-ion-battery-costs-and-market.pdf, Accessed on: May 2, 2019.

Wesley D. Connor received the B.S. degree in mechanical engineering from Rensselaer University, Troy, NY, USA, in 2013. He is currently working toward the Ph.D. degree with the Department of Mechanical Engineering, University of Delaware, Newark, DE, USA. He is currently a Helwig Fellow. His research interests focus on energy impacts of connected and automated vehicles.

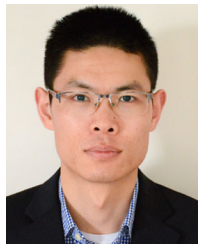

Yongqiang Wang is currently working toward the Ph.D. degree with the Department of Mechanical Engineering, University of Delaware, Newark, DE, USA. His research interests focus on the power management system of hybrid vehicles that improves fuel efficiency and durability, as well as its performance under connected vehicle scenarios.

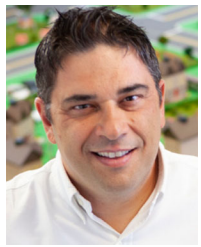

Andreas A. Malikopoulos (Senior Member, IEEE) received the Diploma degree in mechanical engineering from the National Technical University of Athens, Athens, Greece, in 2000, and the M.S. and Ph.D. degrees from the Department of Mechanical Engineering, University of Michigan, Ann Arbor, MI, USA, in 2004 and 2008, respectively. He is the Terri Connor Kelly and John Kelly Career Development Associate Professor with the Department of Mechanical Engineering, University of Delaware (UD), the Director of the Information and Decision Science Laboratory, and the Director of the Sociotechnical Systems Center. Before he joined UD, he was the Deputy Director and the Lead of the Sustainable Mobility Theme of the Urban Dynamics Institute, Oak Ridge National Laboratory, and a Senior Researcher with General Motors Global Research and Development. His research spans several fields, including analysis, optimization, and control of cyber-physical systems; decentralized systems; stochastic scheduling and resource allocation problems; and learning in complex systems. The emphasis is on applications related to sociotechnical systems, energy efficient mobility systems, and sustainable systems. He is currently an Associate Editor for the IEEE TRANSACTIONS ON INTELLIGENT VEHICLES and IEEE TRANSACTIONS ON INTELLIGENT TRANSPORTATION SYSTEMS. He is a member of SIAM, AAAS, and a Fellow of the ASME.

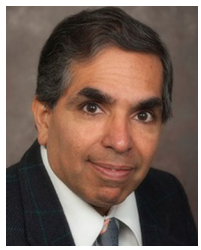

Suresh G. Advani received the Ph.D. degree from the University of Illinois at Urbana-Champaign, Champaign, IL, USA, in 1987. He is George W. Laird Professor of Mechanical Engineering and an Associate Director, Center for Composite Materials, the University of Delaware. He has authored or coauthored more than 300 journal papers and delivered more than 100 invited lectures. He is the Lead Author of a text on *Process Modeling in Composites Manufacturing Processes*. He is a Fellow of American Society of Mechanical Engineers and is the North American Editor for the journal *Composites Part A: Applied Science and Manufacturing*. He recently received the Outstanding Researcher Award for 2015 from American Society of Composites.

Ajay K. Prasad received the Ph.D. degree in mechanical engineering from Stanford University, Stanford, CA, USA, in 1989. He is the Engineering Alumni Distinguished Professor and Chair of the Department of Mechanical Engineering, University of Delaware. His research interests focus on novel materials and systems for automotive fuel cells, renewable hydrogen generation, and hydrogen storage. He co-directs the UD Fuel Cell Bus Program whose goal is to research, build and demonstrate fuel cell/battery hybrid buses and hydrogen refueling stations in Delaware.